

Low-frequency, wideband study of an active repeater, FRB 20240114A, with the GMRT

U. PANDA ¹, J. ROY ¹, S. BHATTACHARYYA ¹, C. DUDEJA ¹ AND S. KUDALE ¹

¹ National Centre for Radio Astrophysics, Tata Institute of Fundamental Research, Pune, Maharashtra, India (PIN: 411007)

ABSTRACT

We report the detection of a total of 135 bursts from a recently discovered active, repeating fast radio burst, FRB 20240114A with the GMRT over a frequency range of 300–750 MHz. The bursts were detected with intrinsic widths ranging from 0.308 to 39.364 ms, a median scattering timescale of 2.059 ms at 400 MHz and 1.372 ms at 650 MHz. The fluences of the detected bursts range from 36.81 mJy ms to 7.47 Jy ms. Both the energy and waiting time distributions of the bursts can be fitted with broken power laws, indicating the presence of two distinct populations of bursts. The energy distributions were modeled via broken power law with $\alpha_1 = -0.62 \pm 0.01$ and $\alpha_2 = -1.98 \pm 0.11$, while the waiting time distribution was modeled via a broken power law with $\alpha_1 = -0.71 \pm 0.01$ and $\alpha_2 = -2.09 \pm 0.09$. Both the energy and waiting time distributions of FRB 20240114A are comparable to high-energy bursts from magnetars, and giant radio pulses from pulsars, indicating that such objects could be likely progenitors.

1. INTRODUCTION

Fast radio bursts (FRBs) are extremely bright, transient, millisecond-scale events seen in the radio sky. Initially discovered quite serendipitously in 2007 (Lorimer et al. 2007), they are now believed to be occurring ubiquitously throughout the Universe, with an estimated sky rate of 525 ± 30 (stat.) $_{-131}^{+142}$ (sys.) bursts sky⁻¹ day⁻¹ (estimated from CHIME’s first FRB catalogue; see Amiri et al. (2021), and the associated erratum). The unusually high values of their dispersion measure (DM) indicated that these were extragalactic events, and this was subsequently confirmed by localizations of several events to their host galaxies (e.g.: Chatterjee et al. (2017); Tendulkar et al. (2017); Bannister et al. (2019); Xu et al. (2022) and many others). Although 941 (as per the TNS database, checked on 15/05/2024) of these events have been detected since their initial discovery, their origins remain a mystery. Their observed flux density, and their large distance from us, imply energies exceeding 10^{22} ergs. Moreover, their timescale of a few milliseconds or more implies an emission region as compact as $\lesssim 30$ km. Thus, the discovery and analysis of more such sources can help provide a deeper insight into their possible progenitors, emission mechanisms, and host environments.

The CHIME/FRB collaboration reported the discovery of an active, repeating FRB, FRB 20240114A, on 26 January 2024 (Shin & CHIME/FRB Collaboration 2024). Since then, several telescopes have conducted follow-up observations on this source, including Parkes/Murriyang (Uttarkar et al. 2024), Westerbork (Ould-Boukattine et al. 2024), FAST (Zhang et al. 2024a,b), Northern Cross (Pellicciari et al. 2024a,b), MeerKAT (Tian et al. 2024), GMRT (Kumar et al. 2024; Panda et al. 2024), Nancay (Hewitt et al. 2024), Allen (Joshi et al. 2024), and others. Since the source was detected at a declination where the CHIME’s beam is much narrower (~ 4 minutes), they inferred a high burst rate. This was subsequently verified by many of the observations above, particularly by a recent observation by FAST (Zhang et al. 2024b), wherein they detected ~ 250 bursts in a single 30-minute epoch. The burst was first potentially associated with one of several galaxy clusters using DESI legacy imaging (O’Connor et al. 2024), and then localized by MeerKAT (Tian et al. 2024) to within an accuracy of ~ 1.5 arcseconds, and by EVN PRECISE (Snelders et al. 2024) to an accuracy of ± 200 milliarcseconds. Both localizations agree within 1σ of one another and indicate that the source is associated with J212739.84+041945.8, a galaxy catalogued in the Sloan Digital Sky Survey (SDSS) with a photometric redshift of $z = 0.42$ (Alam et al. 2015). Recent observations reported in ATel #16613 using the Optical System for Imaging and low-Intermediate-Resolution Integrated

Spectroscopy (OSIRIS) spectrograph at the GTC telescope, gave a spectroscopic redshift of $z = 0.13 \pm 0.0002$, which corresponds to a luminosity distance of $D_L = 610.29$ Mpc. While [Xing & Yu \(2024\)](#) reported the presence of coincident γ -ray emission from the direction of this source using public Fermi LAT data, this was swiftly contradicted by [Principe et al. \(2024\)](#), who reported a non-detection.

In this paper, the detection of multiple bursts from FRB 20240114A with the uGMRT at low frequencies is reported, along with the results from the investigation of various statistical properties of these bursts. In §2, the observations and data processing methodology are described. The results from the analysis are presented in §3, followed by a summary in §4.

2. OBSERVATIONS AND ANALYSIS

We observed FRB 20240114A on two epochs: 25/02/2024 and 14/03/2024. The former observation was carried out for approximately 8 hours, divided into 6 scans, using uGMRT’s Band 4 receivers (550 – 750 MHz). Since the source had already been localised precisely, we chose to trade off our field-of-view for increased sensitivity, by using the uGMRT’s phased array mode, with a phased addition of 22 antennas providing a gain of ~ 7 K/Jy. Two beams were recorded in parallel: a phased array beam with 4096 channels over 200 MHz bandwidth at a time resolution of $81.92 \mu\text{s}$, and another phased array beam, coherently dedispersed on-the-fly to the DM reported by CHIME (527.7 pc cm^{-3} ; see [Shin & CHIME/FRB Collaboration \(2024\)](#)), with 128 channels, over 200 MHz bandwidth at a time resolution of $2.56 \mu\text{s}$. The former beam was incoherently dedispersed and was used to search for single pulses from the FRB, while the latter beam was then used to carry out detailed analyses of the bursts at higher time resolution that were successfully detected. For the second epoch, we observed the source for approximately 4 hours, divided into 4 scans, using uGMRT’s Band 3 and Band 4 receivers simultaneously. We were able to observe the source in both bands at the same time by configuring the uGMRT in sub-array mode, using 10 antennas in Band 3, and 12 in Band 4, which provided a gain of ~ 3.8 K/Jy in both the bands. While this results in a lower sensitivity, it allows for the possibility of simultaneous detections over a wide frequency band. Two beams were recorded in parallel for each sub-array: a phased array beam with 4096 channels over 200 MHz bandwidth, at a time resolution of $163.84 \mu\text{s}$, and a coherently-dedispersed phased array beam, with 512 channels over 200 MHz bandwidth at a time resolution of $20.48 \mu\text{s}$. Simultaneously, visibility data was also recorded for all these observations

with the source 2225–049 used as a bandpass, flux, and gain calibrator, and this calibrator preceded every target scan. We carried imaging analysis using this visibility data with an automated imaging pipeline, which is composed of `flagcal` (for flagging and calibrating GMRT visibilities), `PyBDSF`¹ (for automatic source detection), and `CASA` for deconvolution and self-calibration. We carried two loops of phase-only and final amplitude-phase calibration for self-calibration.

We used the same procedure to search for bursts from both observations. First, we cleaned the data for the radio frequency interference (RFI) using the GMRT Pulsar Tool (`gptool`)². Then, we incoherently dedispersed the data over a DM range of 520 to 535 pc cm^{-3} , while downsampling the data down to a time resolution of $327.68 \mu\text{s}$, using `PRESTO`’s `prepsubband` utility³. After dedispersing the data, we carried out a single pulse search, also using `PRESTO`, with a detection threshold of 5σ . Since the number of candidates obtained was large, we divided them into two separate classes based on signal-to-noise ratio (SNR): high SNR candidates with an $\text{SNR} > 10$, and low SNR candidates with an $\text{SNR} < 10$. The former class of candidates was analysed first, after which the latter class was sifted through. In order to help us judge between actual and spurious candidates, we used `candies`⁴, a program used to extract meaningful features from candidates ([Panda et al. in prep](#)) getting developed for the `SPOTLIGHT`⁵ project. Currently, `candies` constructs two features for each candidate: a dedispersed dynamic spectrum and a DM transform.

Sifting through both classes of candidates mentioned above gave us a total of 119 (73 in the first epoch and 46 in the second) detections in Band 4, and 16 detections in Band 3, making it a total of 135 unique bursts⁶. We haven’t detected any simultaneous bursts in Bands 3 and 4, indicating that the emission from this source is extremely band-limited. For the former observation, we extracted each of the bursts from the corresponding coherently-dedispersed data. We first dedispersed each burst to its detected DM without collapsing the frequency axis via `RollingDedispersion.jl`⁷. We then

¹ <https://github.com/lofar-astron/PyBDSF>

² <https://github.com/chowdhuryaditya/gptool>

³ <https://github.com/scottransom/presto>

⁴ <https://github.com/astrogegwaw/candies>

⁵ <https://spotlight.ncra.tifr.res.in>

⁶ Refer to this link for the gallery listing all bursts, and their observed properties: <https://drive.google.com/drive/folders/1aQKL8C5BR2ENefRbaYbWo4hstaymkU9h?usp=sharing>. The latter are stored as CSV files, for easy access.

⁷ <https://github.com/astrogegwaw/RollingDedispersion.jl>

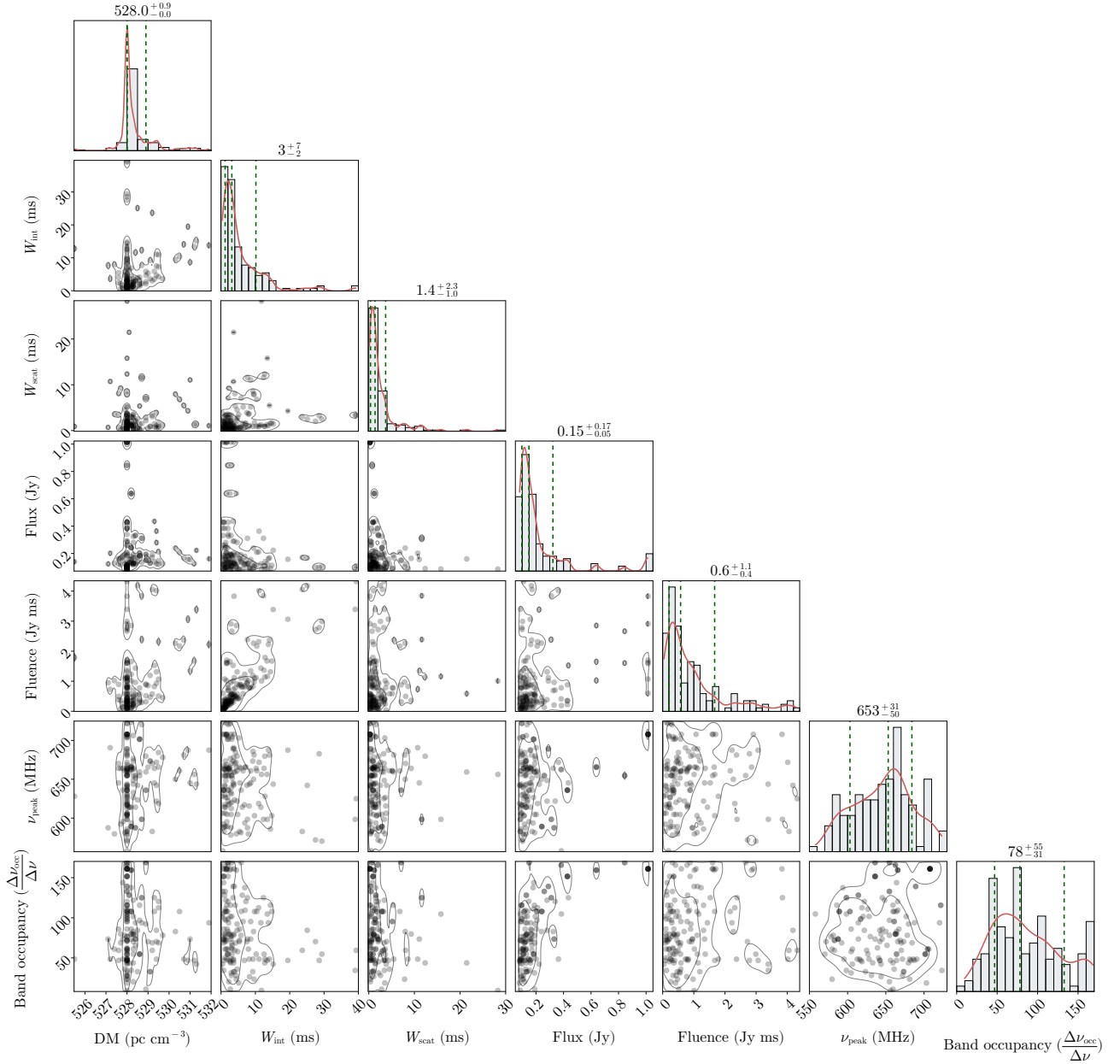


Figure 1. Distributions of fitted parameters for all bursts detected in the Band 4 observations on 25/02/2024 and 14/03/2024, plotted as a corner plot. This allows us to see the correlations, or their absence thereof, between different parameters. Bursts detected in Band 3 were excluded, since including them would have introduced deviation into the distribution of spectral parameters, such as the peak frequency or the band occupancy.

downsampled all bursts to 128 channels along frequency. For the data recorded on 25/02/2024, we downsampled the data to a time resolution of 40.96 μs , 163.84 μs , or 327.68 μs , depending on whether the SNR of the burst was > 25 , between 10 and 25, or < 10 respectively. For the data recorded on 14/03/2024, we downsampled everything to 655.36 μs , in order to compensate for the SNR loss due to the use of uGMRT’s subarray mode. Then, we corrected for the bandpass via a median normalisation, and stored all bursts as `*.npz` files. Further analysis was carried out using `burfi` (Bhattacharyya et al. in prep), an analysis toolkit getting developed for the SPOTLIGHT project. It independently fits each burst’s profile and spectrum, while taking the presence of multiple burst components and band-limited emission into account. For fitting each burst component, we assume that each component is: 1) an intrinsically normalised Gaussian, and 2) scattered equally and isotropically from a thin screen (that is, all components have the same scattering timescale, τ_s). Since the data was coherently dedispersed, we ignored the presence of any residual DM smearing. The above assumptions lead to the following analytical expression for each component (adapted from McKinnon (2014)):

$$f(t, \tilde{\mathbf{x}}) = b + \frac{F}{2\tau_s} \times \exp\left(\frac{\sigma^2}{2\tau_s^2}\right) \times \exp\left(-\frac{t-\mu}{\tau_s}\right) \times \text{erfc}\left[-\frac{1}{\sqrt{2}}\left(\frac{t-\mu}{\sigma} - \frac{\sigma}{\tau_s}\right)\right] \quad (1)$$

where t is time, $\tilde{\mathbf{x}}$ is the parameter vector, F is the burst fluence or the area under the pulse, μ is the mean, σ is the standard deviation, τ_s is the scattering timescale, `erfc` is the complementary error function, defined as `erfc(x) = 1 - erf(x)`, and b is the baseline offset. We assume all components to have the same τ_s , as well as the same baseline offset b .

For spectral fitting, we isolated the frequency channels where the burst was present (that is, its emission band). This was done by first isolating sub-bands where the emission was highest, collapsing each of them, and then calculating the SNR via convolution with a boxcar of the same width as the detected burst, to evaluate whether it is present in that sub-band. This SNR calculation was carried out using `spyden`⁸. Sub-bands where the burst was present with an SNR greater than a certain threshold were merged together, and then the spectrum was fit only over this region. For this fit, we used a simple Gaussian model. All fits were carried out using `scipy’s curve_fit`.

3. RESULTS AND DISCUSSIONS

We observed 73 bursts in the first epoch and 46 in the second epoch in Band 4, which implies a burst rate of 11.2 bursts hr^{-1} above a fluence of 36.8 mJy ms, and 14.2 bursts hr^{-1} above a fluence of 0.32 Jy ms, respectively. After obtaining post-fit parameters from bursts, and individual burst components, as outlined in § 2, the next step was to look at their statistics. A bird’s-eye view of the statistics for all bursts detected in Band 4 is given via Figure 1. In this figure we excluded the bursts detected in Band 3 since they were less in number and would have introduced deviations into the distributions of spectral parameters, such as the peak emission frequency, or the band occupancy. From the plot, we can see that the DM of the bursts is tightly constrained around the median value of $\text{DM}_{\text{med}} = 528.0 \text{ pc cm}^{-3}$, and ranges from 525.5 to 531.9 pc cm^{-3} . The intrinsic width and the scattering timescale range from 0.31 ms to 39.36 ms, and 0.12 ms to 28.29 ms, respectively. We also observed a wide fluence range of 36.82 mJy ms to 7.47 Jy ms. The distributions for the intrinsic and scattering widths, and the flux density and fluence of the bursts, are all long-tailed, while the ones for the peak emission frequency and the band occupancy of the bursts are flat. This indicates that: 1) while the former four parameters are clustered around their median values, there are a significant number of bursts for which these deviate, and 2) the latter two parameters are mostly unconstrained, which is quite typical of repeating FRBs. In Figure 2, we plot the absolute deviation of these burst parameters from their median values. Note that we have included the bursts detected in Band 3, and thus have calculated the median peak emission frequency for them separately. The different colours denote different observation epochs. The median scattering timescale estimated for 14/03/2024 for Band 3 and Band 4 is 2.06 ms and 3.25 ms, respectively. The median DM and fluence values measured for both bands are 528.2 pc cm^{-3} , 1.13 Jy ms for Band 3, and 528.0 pc cm^{-3} , 1.19 Jy ms for Band 4. The median value of the emission bandwidth estimated for both the bands is 73.438 MHz for Band 3, and 59.375 MHz for Band 4. Though we observed an offset between the scattering timescale, median DM, fluence and emission bandwidth values between the two bands, we cannot confirm the significance of this offset, since we detected relatively fewer bursts in our dual-frequency sub-array observation. For both bands recorded on 14/03/2024, one can see that the deviations were highest across all parameters, except for the flux density. This can further be confirmed by looking at the corresponding plot for the fluence of the bursts, where, once again, one can

⁸ <https://bitbucket.org/vmorello/spyden>

see larger deviations for the 14/03/2024 epochs. While we did detect fewer bursts on 14/03/2024 due to the observation mode, we can still see that these bursts had greater DM offsets, and were less bright, intrinsically wider, and more scattered, compared to those detected on 25/02/2024. These deviations could possibly imply an evolution in the activity of FRB 20240114A in the 18 days between 25/02/2024 and 14/03/2024, and might explain the extreme activity detected by other telescopes around the same time as the latter epoch, such as FAST (Zhang et al. 2024b).

3.1. Isotropic Energy Distribution

The isotropic energy distribution of the bursts is shown in Figure 3A. The isotropic energy released from a burst was calculated using the following equation (Aggarwal 2021):

$$E = 4\pi \times \left(\frac{D_L}{\text{cm}}\right)^2 \left(\frac{F}{\text{Jy s}}\right) \left(\frac{\Delta\nu_{\text{occ}}}{\text{Hz}}\right) \times 10^{-23} \text{ erg}, \quad (2)$$

where D_L is the luminosity distance (610.29 Mpc for $z = 0.13$ for FRB 20240114A, taken from ATel #16613), F is the fluence, $\Delta\nu_{\text{occ}}$ is the band occupancy, and E is the isotropic energy of the burst. The energy distributions of both high-energy bursts from magnetars, as well as giant pulses from pulsars, have been found to be well-modeled by a power law of the form $dN \propto E^\alpha dE$. For instance, Göğüş et al. (1999, 2000) found that the bursts from the magnetar SGR 1806–20 were well-described by power laws with indices -1.43 , -1.67 , and -1.76 , and bursts from the magnetar SGR 1900+14 were well described by a single power law with an index of -1.66 . Similarly, Bera & Chengalur (2019) found a spectral index of ≈ -3.0 for giant pulses from the Crab pulsar. Such examples have motivated similar modeling to be carried out for FRBs. Since we could see a break in the distribution, we modeled it using a broken power law (BPL), fitting the former part of the distribution using a power law with slope $\alpha_1 = -0.62 \pm 0.01$, and the latter part of the distribution using a power law with slope $\alpha_2 = -1.98 \pm 0.11$, with a break between both distributions at $E_{\text{break}} = (6.24 \pm 0.25) \times 10^{37}$ ergs. The slope of the latter distribution resembles that of the Crab pulsar’s giant pulses (for example, see Mickaliger et al. (2012)).

3.2. Waiting Time Distribution

The waiting time distribution of the bursts is plotted in Figure 3B. The distribution is clearly bimodal, as can be seen via the kernel density estimate (KDE) plotted over it. Note that the x -axis is logarithmic.

We can go further and look at the cumulative waiting time distribution as well, plotted in Figure 3C, which has once again been modeled by using a broken power law (BPL). The former distribution was fitted using a power law with slope $\alpha_1 = -0.71 \pm 0.01$, while the latter was fitted using a power law with slope $\alpha_2 = -2.09 \pm 0.09$, with a break between the two distributions at $t_{\text{break}} = 413.68 \pm 11.62$ seconds. As Aschwanden & McTiernan (2010) showed, a non-stationary Poisson process can lead to a power law waiting time distribution, which plateaus towards shorter waiting times. A smaller value of the power law index typically implies a more rapidly varying burst rate (Aschwanden & McTiernan 2010). A broken power law indicates the presence of two distinct populations, with the burst rate for the former varying much more rapidly and intermittently than the latter. This aligns with observations since the former distribution represents burst profile components, sub-bursts, or very close by, but independent, bursts.

3.3. Persistent Radio Source

From the preliminary analysis, ATel #16613 classified the host of FRB 20240114A as a dwarf star-forming galaxy, and noted that its similarity to the hosts of FRB 20121102A and 20190520B. Both FRBs are highly active repeaters, and have been associated with a persistent radio source (PRS). However, a search for such a source in archival radio survey data by the authors of ATel #16613 yielded nothing, allowing them to place a 3σ upper limit of $300 \mu\text{Jy}$, using FIRST survey data, taken at 1.5 GHz. A more stringent 5σ upper limit of $140 \mu\text{Jy}$ had already been placed earlier by Kumar et al. (2024) using the uGMRT. Through our imaging analysis (for details see § 2), we also did not find any significant detection. The RMS in the region around the FRB’s location is $24.8 \mu\text{Jy} / \text{beam}$; hence, we set the upper detection limit on any continuum emission coincident with this FRB to $124 \mu\text{Jy}$, with a 5σ significance. Note that this is the most stringent constraint on the PRS, and is ~ 1.5 to 2 times fainter than the spatially coincident PRS detected for FRB 20121102A ($180 \mu\text{Jy}$) or 20190520B ($260 \mu\text{Jy}$) (Chatterjee et al. 2017; Niu et al. 2022).

4. SUMMARY

We detected a sample of 135 bursts from FRB 20240114A in two epochs observing over a span of 300–750 MHz. The results from our subsequent analysis of the distributions of the post-fit parameters obtained from this sample can be summarised as follows:

- The dispersion measure of the bursts is tightly constrained around the median value of $DM =$

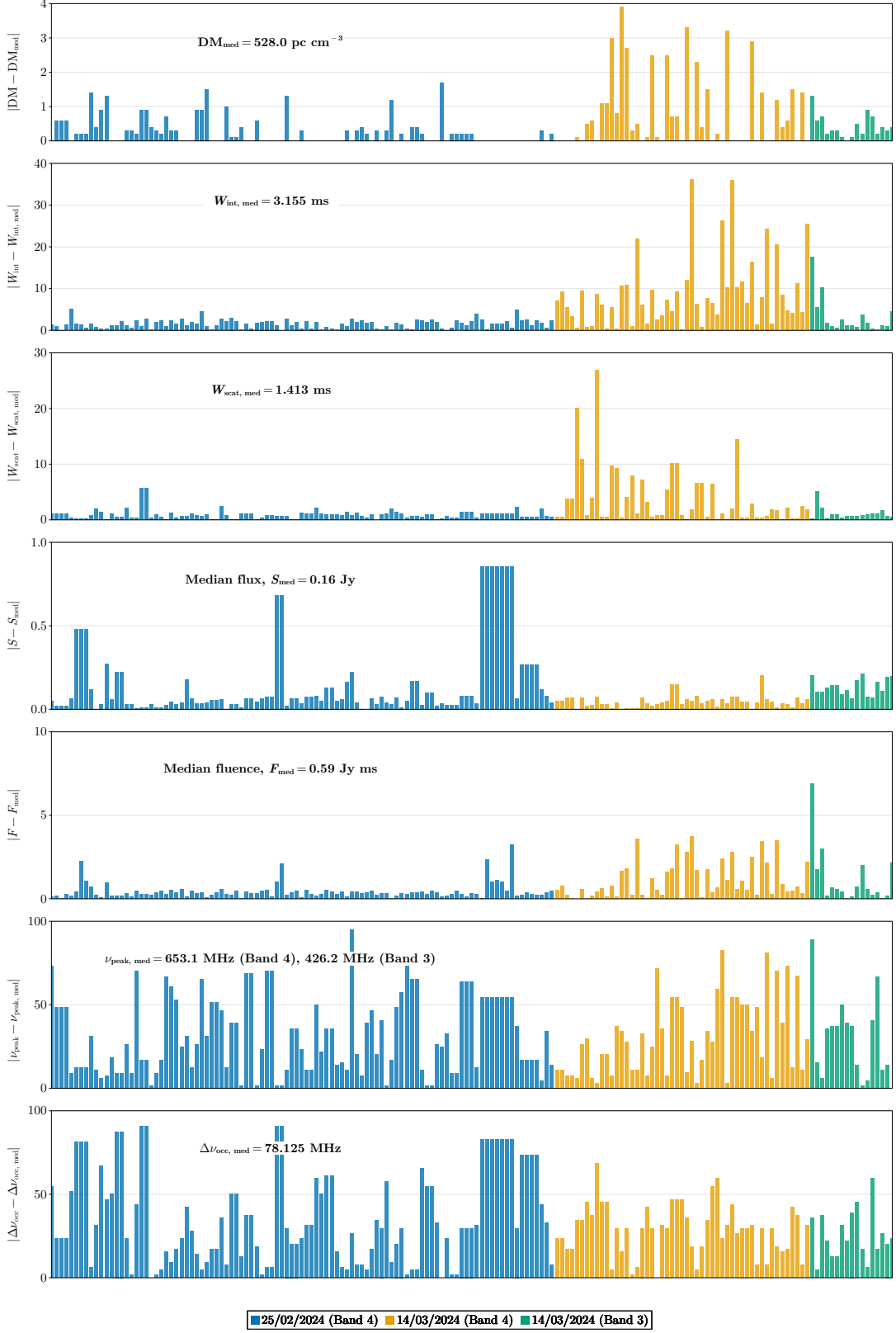


Figure 2. Absolute deviations of all post-fit burst parameters from their median values. The color indicates different observation epochs. From the plot, it can be clearly seen that the greatest deviations are seen for the data recorded in Band 4 on 14th March 2024. For the peak frequency, we calculate the absolute deviations from the median separately for Band 3 and Band 4 bursts.

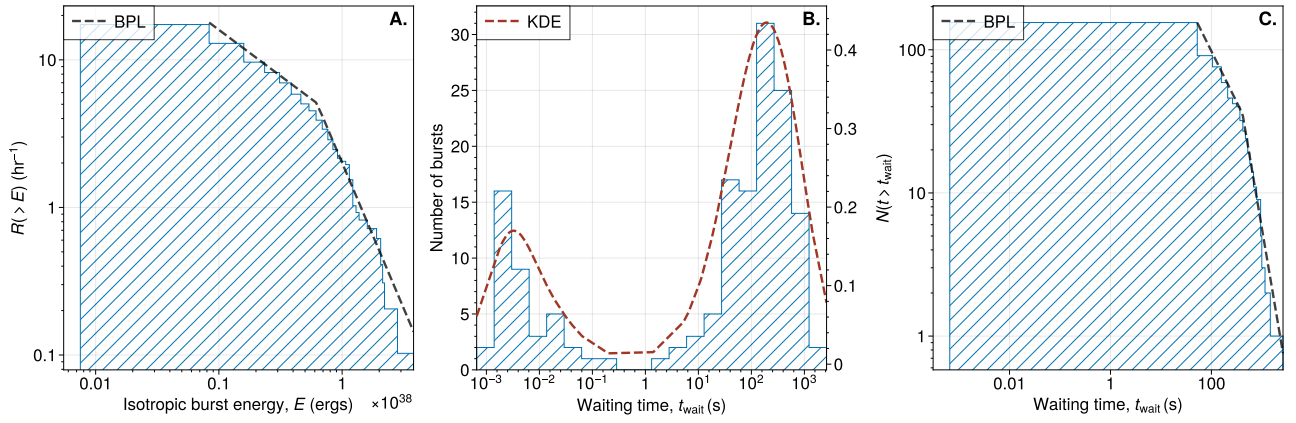


Figure 3. **A.** The cumulative isotropic energy distribution for all bursts. We fit this distributions with a broken power law (BPL) with $\alpha_1 = -0.62 \pm 0.01$ and $\alpha_2 = -1.98 \pm 0.11$, which has been plotted as well. The break between the two power laws occurs at $E_{\text{break}} = (6.24 \pm 0.25) \times 10^{37}$ ergs. **B.** The waiting time distribution and **C.** the cumulative waiting time distribution for all bursts. For the former, we have plotted the kernel density estimate (KDE), bringing the bi-modality of the distribution to the forefront. The same bi-modality can be seen in **C.**, and has been fitted with a broken power law with $\alpha_1 = -0.71 \pm 0.01$ and $\alpha_2 = -2.09 \pm 0.09$. The break occurs at $t_{\text{break}} = 413.68 \pm 11.62$ seconds.

528 pc cm⁻³. Their peak frequency and band occupancy vary widely, a behaviour typical of repeating FRBs. A majority of the bursts were narrow, scattered, and faint.

- A possible change of activity state between two epochs separated by 18 days was observed, in terms of the temporal evolution of the DM, intrinsic width, scattering timescale, and fluence of the bursts. Also, a possible frequency-dependent evolution of some of the burst properties was seen in our dual-frequency observation.
- Both the energy and waiting time distributions were well-fit by a broken power law. This once again implied the presence of two distinct populations of bursts. A flatter slope (-0.71 ± 0.01) in the waiting time distribution, along with a steeper

slope (-1.98 ± 0.1) in the energy distribution, points to a small population of bright, closely clustered, and intermittent bursts, overlaid on a larger population of faint bursts being regularly emitted by this source.

1 We gratefully acknowledge the Department of Atomic
2 Energy, Government of India, for its assistance under
3 project No. 12-R&D-TFR-5.02-0700. Furthermore, we
4 are grateful to the GMRT Operations Team for the
5 prompt approval and scheduling of the DDT observa-
6 tions that allowed us to probe this FRB while it was in
7 its active state, and the staff of the GMRT that made
8 these observations possible. GMRT is run by the Na-
9 tional Centre for Radio Astrophysics of the Tata Insti-
10 tute of Fundamental Research.

REFERENCES

- Aggarwal, K. 2021, *ApJL*, 920, L18, doi: [10.3847/2041-8213/ac2a3a](https://doi.org/10.3847/2041-8213/ac2a3a)
- Alam, S., Albareti, F. D., Allende Prieto, C., et al. 2015, *The Astrophysical Journal Supplement Series*, 219, 12, doi: [10.1088/0067-0049/219/1/12](https://doi.org/10.1088/0067-0049/219/1/12)
- Amiri, M., Andersen, B. C., Bandura, K., et al. 2021, *ApJS*, 257, 59, doi: [10.3847/1538-4365/ac33ab](https://doi.org/10.3847/1538-4365/ac33ab)
- Aschwanden, M. J., & McTiernan, J. M. 2010, *ApJ*, 717, 683, doi: [10.1088/0004-637X/717/2/683](https://doi.org/10.1088/0004-637X/717/2/683)
- Bannister, K. W., Deller, A. T., Phillips, C., et al. 2019, *Science*, 365, 565, doi: [10.1126/science.aaw5903](https://doi.org/10.1126/science.aaw5903)
- Bera, A., & Chengalur, J. N. 2019, *Monthly Notices of the Royal Astronomical Society: Letters*, 490, L12, doi: [10.1093/mnrasl/slz140](https://doi.org/10.1093/mnrasl/slz140)
- Chatterjee, S., Law, C. J., Wharton, R. S., et al. 2017, *Nature*, 541, 58, doi: [10.1038/nature20797](https://doi.org/10.1038/nature20797)
- Gögüş, E., Woods, P. M., Kouveliotou, C., et al. 1999, *ApJ*, 526, L93, doi: [10.1086/312380](https://doi.org/10.1086/312380)
- . 2000, *ApJ*, 532, L121, doi: [10.1086/312583](https://doi.org/10.1086/312583)
- Hewitt, D. M., Huang, J., Hessels, J. W. T., et al. 2024, *The Astronomer’s Telegram*, 16597, 1. <https://ui.adsabs.harvard.edu/abs/2024ATel16597...1H>
- Joshi, P., Medina, A., Earwicker, J. T., et al. 2024, *The Astronomer’s Telegram*, 16599, 1. <https://ui.adsabs.harvard.edu/abs/2024ATel16599...1J>
- Kumar, A., Maan, Y., & Bhusare, Y. 2024, *The Astronomer’s Telegram*, 16452, 1. <https://ui.adsabs.harvard.edu/abs/2024ATel16452...1K>
- Lorimer, D. R., Bailes, M., McLaughlin, M. A., Narkevic, D. J., & Crawford, F. 2007, *Science*, 318, 777, doi: [10.1126/science.1147532](https://doi.org/10.1126/science.1147532)
- McKinnon, M. M. 2014, *Publications of the Astronomical Society of the Pacific*, 126, 476, doi: [10.1086/676975](https://doi.org/10.1086/676975)
- Mickaliger, M. B., McLaughlin, M. A., Lorimer, D. R., et al. 2012, *ApJ*, 760, 64, doi: [10.1088/0004-637X/760/1/64](https://doi.org/10.1088/0004-637X/760/1/64)
- Niu, C.-H., Aggarwal, K., Li, D., et al. 2022, *Nature*, 606, 873, doi: [10.1038/s41586-022-04755-5](https://doi.org/10.1038/s41586-022-04755-5)
- O’Connor, B., Bhardwaj, M., & Palmese, A. 2024, *The Astronomer’s Telegram*, 16426, 1. <https://ui.adsabs.harvard.edu/abs/2024ATel16426...1O>
- Ould-Boukattine, O. S., Hessels, J. W. T., Kirsten, F., et al. 2024, *The Astronomer’s Telegram*, 16432, 1. <https://ui.adsabs.harvard.edu/abs/2024ATel16432...1O>
- Panda, U., Bhattacharyya, S., Dudeja, C., Kudale, S., & Roy, J. 2024, *The Astronomer’s Telegram*, 16494, 1. <https://ui.adsabs.harvard.edu/abs/2024ATel16494...1P>
- Pellicciari, D., Geminardi, A., Bernardi, G., et al. 2024a, *The Astronomer’s Telegram*, 16434, 1. <https://ui.adsabs.harvard.edu/abs/2024ATel16434...1P>
- . 2024b, *The Astronomer’s Telegram*, 16547, 1. <https://ui.adsabs.harvard.edu/abs/2024ATel16547...1P>
- Principe, G., Di Lalla, M. N. N., Omodei, N., et al. 2024, *The Astronomer’s Telegram*, 16602, 1. <https://ui.adsabs.harvard.edu/abs/2024ATel16602...1P>
- Shin, K., & CHIME/FRB Collaboration. 2024, *The Astronomer’s Telegram*, 16420, 1. <https://ui.adsabs.harvard.edu/abs/2024ATel16420...1S>

- Snelders, M. P., Bhandari, S., Kirsten, F., et al. 2024, The Astronomer’s Telegram, 16542, 1. <https://ui.adsabs.harvard.edu/abs/2024ATel16542...1S>
- Tendulkar, S. P., Bassa, C. G., Cordes, J. M., et al. 2017, ApJL, 834, L7, doi: [10.3847/2041-8213/834/2/L7](https://doi.org/10.3847/2041-8213/834/2/L7)
- Tian, J., Pastor-Marazuela, I., Stappers, B., et al. 2024, The Astronomer’s Telegram, 16446, 1. <https://ui.adsabs.harvard.edu/abs/2024ATel16446...1T>
- Uttarkar, P. A., Kumar, P., Lower, M. E., & Shannon, R. M. 2024, The Astronomer’s Telegram, 16430, 1. <https://ui.adsabs.harvard.edu/abs/2024ATel16430...1U>
- Xing, Y., & Yu, W. 2024, The Astronomer’s Telegram, 16594, 1. <https://ui.adsabs.harvard.edu/abs/2024ATel16594...1X>
- Xu, H., Niu, J. R., Chen, P., et al. 2022, Nature, 609, 685, doi: [10.1038/s41586-022-05071-8](https://doi.org/10.1038/s41586-022-05071-8)
- Zhang, J., Zhu, Y., Cao, S., et al. 2024a, The Astronomer’s Telegram, 16433, 1. <https://ui.adsabs.harvard.edu/abs/2024ATel16433...1Z>
- Zhang, J., Wu, Q., Cao, S., et al. 2024b, The Astronomer’s Telegram, 16505, 1. <https://ui.adsabs.harvard.edu/abs/2024ATel16505...1Z>